Copy 245
RM E51125

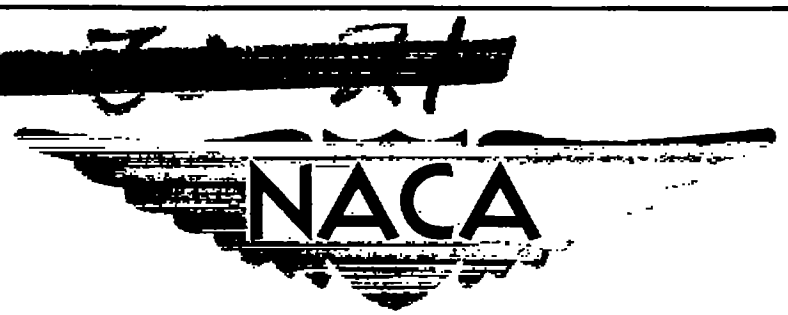

RESEARCH MEMORANDUM

FLOW SEPARATION AHEAD OF A BLUNT AXIALLY SYMMETRIC BODY AT MACH NUMBERS 1.76 TO 2.10

By W. E. Moeckel

Lewis Flight Propulsion Laboratory
Cleveland, Ohio

NATIONAL ADVISORY COMMITTEE
FOR AERONAUTICS

WASHINGTON
December 12, 1951

NATIONAL ADVISORY COMMITTEE FOR AERONAUTICS

RESEARCH MEMORANDUM

FLOW SEPARATION AHEAD OF A BLUNT AXIALLY SYMMETRIC BODY AT MACH NUMBERS 1.76 TO 2.10

By W. E. Moeckel

SUMMARY

The pressure distribution and drag of a spherical-nosed axially symmetric body with slender rods projecting upstream of the nose were determined at Mach numbers of 1.76, 1.93, and 2.10. The upstream projection distance of the rods was varied over a wide range to study the changes in the character of the flow separation and to determine the variation of drag and pressure distribution with rod tip projection.

For small tip projections, the flow separated near the tip of the rod, whereas for larger tip projections, separation took place on the rod surface. For most rod lengths at all Mach numbers, the drag coefficient was between 0.35 and 0.60. Minimum drags were obtained with rod tip projections equal to about three times the nose radius.

INTRODUCTION

An investigation of flow separation ahead of two-dimensional blunt bodies mounted on a flat plate was reported in reference 1. It was found that, for a certain range of body thicknesses (relative to initial boundary-layer thickness), wedge-shaped separation regions formed ahead of the body. The pressures in this dead-air region could be predicted by a simple analysis. As the thickness of the body was increased, the steady wedge-type separation was replaced by an unsteady flow which appeared to oscillate between separation from the surface of the plate and separation from the leading edge.

The present investigation was undertaken to determine whether separation phenomena ahead of axially symmetric blunt bodies are similar to those observed with two-dimensional bodies, and whether a range of initial boundary-layer thicknesses exists for which the analysis of reference 1 is applicable. The drag reduction resulting from flow separation ahead of the body was determined in the Mach number range investigated, and was compared with analytical values. This investigation was conducted at the NACA Lewis laboratory.

DESCRIPTION OF MODEL

A sketch of the spherical-nose body used is shown in figure 1, together with significant dimensions and notations. The nose was fitted with bushings through which circular rods of radii 0.1R, 0.17R, and 0.25R were inserted to provide an initial boundary layer. Each rod had a conical tip of 40° included angle. The projection distance of the tip of the rods upstream of the nose L_1 could be varied during tunnel operation by manipulation of a flexible extension of the rod outside the tunnel. For some of the tests, a 1/4-inch strip of carborundum dust was placed around the rods immediately downstream of the conical tips to induce transition of the boundary layer; but no attempt was made to determine whether a turbulent boundary layer was actually produced.

Static-pressure orifices were located at 10° intervals on the spherical portion of the nose from $\theta = 0°$ to $\theta = 80°$. For θ greater than 80°, the contour of the body becomes parabolic. Pressure orifices in the parabolic portion of the body were not used, because only the drag of the spherical nose was desired.

The experiments were conducted in the NACA Lewis 18- by 18-inch tunnel, which has a test-section Mach number of 1.9 and a Reynolds number of 3.24×10^6 per foot. In order to obtain other Mach numbers, the body was mounted on a flat plate whose angle of attack could be varied. In this manner, the models were tested at Mach numbers of 1.76, 1.93, and 2.10. Schlieren photographs were taken of the flow patterns corresponding to each tip projection, rod radius, and Mach number.

RESULTS AND DISCUSSION

Schlieren Observations

A typical sequence of flow transformations resulting when the tip projections of the rods were increased is shown in figure 2. With the tip of the rod only a short distance upstream of the nose (fig. 2(a)), conical separation from the shoulder of the rod is already apparent. The detached shock obtained with zero tip projection is replaced by a conical shock followed by a curved shock which appears to originate slightly upstream of the point of contact of the separated-flow region with the body. As the tip projection is increased (figs. 2(b), 2(c), and 2(d)), the conical separation angle decreases until a critical tip projection is reached. For tip projections greater than the critical value, transition from separation at the shoulder to separation on the surface of the rod takes place (fig. 2(e)). Further increases in tip projection appear to have little effect on the flow pattern near the nose, except that the shocks and the separation boundary

become more distinct for large rod extensions (figs. 2(f) to 2(i)). The point of origin of the second shock remains almost unchanged throughout the transformations. The presence of this shock indicates that the separation boundary is not precisely tangent to the spherical nose and also that the flow remains supersonic outside the shear layer.

Schlieren photographs taken at other Mach numbers showed the same succession of transformations as those of figure 2 and are therefore not reproduced. There were qualitative differences, however, in schlieren photographs taken with and without the carborundum strip on the rod. Figure 3 shows the sequence of transformations obtained with the same rod and Mach number as those of figure 2, but with the strip of carborundum placed immediately downstream of the rod shoulder. The chief differences are the tip projection for which transition from one type of separation to the other takes place and the sharper image of the shocks and separation boundary obtained with large tip projections.

The sequence of events shown in figures 2 and 3 is in some ways similar to that obtained in reference 1 with blunt two-dimensional bodies of various thicknesses mounted downstream of the leading edge on a flat plat. For small values of the ratio of body thickness to projecting plate length (b/L) separation occurred on the surface of the plate downstream of the leading edge. As the body thickness was increased beyond a critical value, unsteady transition from separation on the surface to separation from the leading edge was observed. For the maximum values of b/L investigated, however, no steady separation from the leading edge was obtained, although the pressures in the separation region were comparable with those expected for this type of separation. One of the chief qualitative differences noted between the two-dimensional and the three-dimensional phenomena is that the change from one type of separation to the other was accompanied by oscillatory flow in the two-dimensional case, whereas no unsteady flow configurations were observed in the present investigation.

Pressure Distributions

Pressure distributions over the nose of the body from $\theta = 10^\circ$ to $\theta = 80^\circ$ are shown in figure 4 for a Mach number of 1.93. The effect of tip projection, rod radius, and the transition strip on pressure distribution was qualitatively similar at other Mach numbers. For each rod radius, the peak pressure coefficient decreases steadily and shifts toward larger θ as the tip projection is increased from zero. The peaks reach a minimum at or near the tip projection for which the origin of separation begins to change from the shoulder of the rod to the downstream surface. As the tip projection is increased beyond this value, the peak coefficient increases toward a maximum

and shifts gradually toward smaller θ. Further increases in tip projection result in a flattening of the curves with little change in the pressures near $\theta = 10^\circ$ and $\theta = 80^\circ$. This flattening indicates a trend toward truly conical separation, for which a constant static pressure over the portion of the nose in the separation region would be expected.

The pressure distribution obtained in a previous investigation for a spherical nose without projections ($R/L_1 = \infty$) is shown in figure 4(a) for comparison. Although the pressures for small θ are much higher without projections than with even a short projection, the expansion at large θ was more rapid for the body without projections. The less rapid expansion with projecting rods is probably associated with the second shock observed in figures 2 and 3 downstream of the conical shock.

Drag Coefficients

Pressure drag coefficients as a function of tip projection were obtained by numerical integration of the pressure-distribution curves of figure 4, and similar curves for the other Mach numbers. In order to obtain a drag coefficient corresponding to a hemispherical nose, the assumption was made that the pressure coefficient between $\theta = 0^\circ$ and $\theta = 80^\circ$ was independent of the form of the body for θ greater than 80°. The pressure coefficient curves were then extrapolated to $C_p = 0$ at $\theta = 90^\circ$. This extrapolation agrees approximately with the measured pressure coefficients on the parabolic portion of the body, where overexpansion to negative pressure coefficients occurred near $\theta = 90^\circ$. Since the pressure coefficient at $\theta = 80^\circ$ is almost independent of tip projection, and since the projection area of a spherical nose between $\theta = 80^\circ$ and $\theta = 90^\circ$ is only 3 percent of the total, no appreciable error was introduced by this extrapolation. The theoretical drag corresponding to a 40°-included-angle cone with radius equal to the rod radius was added to the drag coefficient obtained from the pressure distributions to represent the contribution of the rods to the pressure drag of the nose. Since the cross sections of the rods were quite small relative to the cross section of the nose, the drag contributions of the tip cones were also small. No attempt was made to determine the friction drag of the configuration; it was indicated in reference 1, however, that this drag should be of the same magnitude as the friction drag of a solid body with the nose form of the separation region.

The resulting drag coefficients are shown as functions of R/L_1 in figure 5 for each Mach number investigated. The variation of drag with tip projection follows the same trend as that noted for the peaks of the pressure distribution curves of figure 4. A minimum drag coefficient is obtained at the tip projection for which the change from separation at the shoulder to separation on the downstream surface of the rod begins. Larger tip projections (smaller R/L_1) result in an increase in drag followed by a more or less steady decrease as R/L_1 becomes very small. For a Mach number M_0 of 2.10 (fig. 5(c)) the drag rise appears to occur in two steps between which C_D is almost constant. At this Mach number the final decrease in C_D as R/L_1 approaches zero apparently starts at values of R/L_1 less than 0.04. Because of vibration of the projecting rod at very large tip projection, values of R/L_1 less than 0.04 could be obtained only with the largest rod used. Hence, the final decrease in C_D as $R/L_1 \rightarrow 0$ was obtained at this Mach number only for $a/R = 0.25$. The minimum drag at each Mach number corresponds approximately to the theoretical drag of a 21° half-angle cone and is less than half of the drag of a spherical nose in a uniform supersonic stream.

DISCUSSION OF RESULTS

In reference 1, the following relationship was derived between the body-thickness ratio and the conical separation angle when separation occurs on the rod surface:

$$\frac{b}{L} = \frac{\frac{2}{\beta}\frac{a}{b} T_c \tan \lambda_c}{\frac{\eta}{\eta - 1} + \frac{2}{\beta}\frac{a}{b} T_c} \tag{1}$$

where T_c is a function of λ_c defined in reference 1, β is a factor of proportionality between the friction coefficient on a solid cone and the friction coefficient on a solid wedge, and η is the exponent of the Reynolds number in the formula for the friction coefficient on a flat plate. The quantities b, a, λ_c, and L are defined in figure 1, from which the following relations are evident:

$$\begin{aligned} b &= R \cos \lambda_c \\ L &= L_1 + R(1 - \sin \lambda_c) \end{aligned} \tag{2}$$

Equation (1) was derived under the following assumptions: (a) The flow separation results in a truly conical dead-air region in which the pressure is constant, and the dead-air boundary is tangent to the body surface; and (b) the change in momentum thickness along the boundary of the dead-air region is proportional to that along a solid cone having the same angle as the dead-air region. From the pressure-distribution curves of figure 4, it is apparent that the conditions assumed for the analysis were not obtained experimentally, although a tendency toward constant pressure in the separation region is evident as the tip projection becomes very large. The fact that the pressure was not constant in the separated region may be due to vortical motions set up by the entrainment of air by the shear layer over the separated region. Such entrainment would require an inflow of air from downstream and may account for the second shock observed near the point of contact of the separated region with the body contour. A reversed flow near the surface at this point could result in a deflection of the air moving downstream, with a consequent shock wave.

The experimental drag coefficients are compared in figure 5 with analytical values corresponding to conical separation from the tip of the rod and to conical separation on the rod surface as given by equations (1) and (2). For small tip projections (large R/L_1) the experimental drag coefficients tend toward the curve corresponding to conical separation from the tip, while for very large tip projections (small R/L_1) the experimental drag coefficients decrease in a manner similar to that predicted by equations (1) and (2). For most tip projections, however, the experimental drag coefficients fail to agree with either of the analytical curves. In particular, the transition from separation on the rod surface to separation from the tip is not accompanied by the large change in drag coefficient predicted in reference 1. In this respect the axially symmetric case differs appreciably from the two-dimensional case, where relatively large changes in pressure coefficient were noted in the separated region during the change in position of separation (reference 1).

The fact that the experimental drag coefficients for values of R/L_1 between 0.50 and 1.0 are higher than those predicted on the basis of conidal separation from the rod tip is probably associated with the circulatory motions in the separated region and with the resulting second shock. The qualitative behavior of the flow for large values of R/L_1, and also for very small values of R/L_1, is therefore reasonably clear. No explanation is yet possible, however, for the behavior of the flow for intermediate values of R/L_1. In particular, the quantities that determine when transition from tip separation to surface separation will occur have not been established, and the reasons for the changes in drag coefficient resulting from changes in the rod radius or from the use of artificial roughness are not known.

CONCLUDING REMARKS

Investigation of the flow past a spherical-nosed body with projecting rods indicates that pressure drag coefficients between 0.35 and 0.60 are obtained at Mach numbers between 1.76 and 2.10 and for rod lengths between 2 and 20 times the nose radius. The minimum drag at each Mach number corresponded approximately to the drag of a 21° half-angle solid cone, and was obtained with a rod length about three times the nose radius. This rod length corresponded to the maximum value for which separation from the tip of the rod occurred. For larger tip projections, the drag coefficient remained much lower than predicted by the conical-separation analysis of reference 1. The discrepancy is believed to be due chiefly to vortical motions in the separated region, which were assumed to be negligible in the analysis of reference 1.

Lewis Flight Propulsion Laboratory
National Advisory Committee for Aeronautics
Cleveland, Ohio

REFERENCE

1. Moeckel, W. E.: Flow Separation Ahead of Blunt Bodies at Supersonic Speeds. NACA TN 2418, 1951.

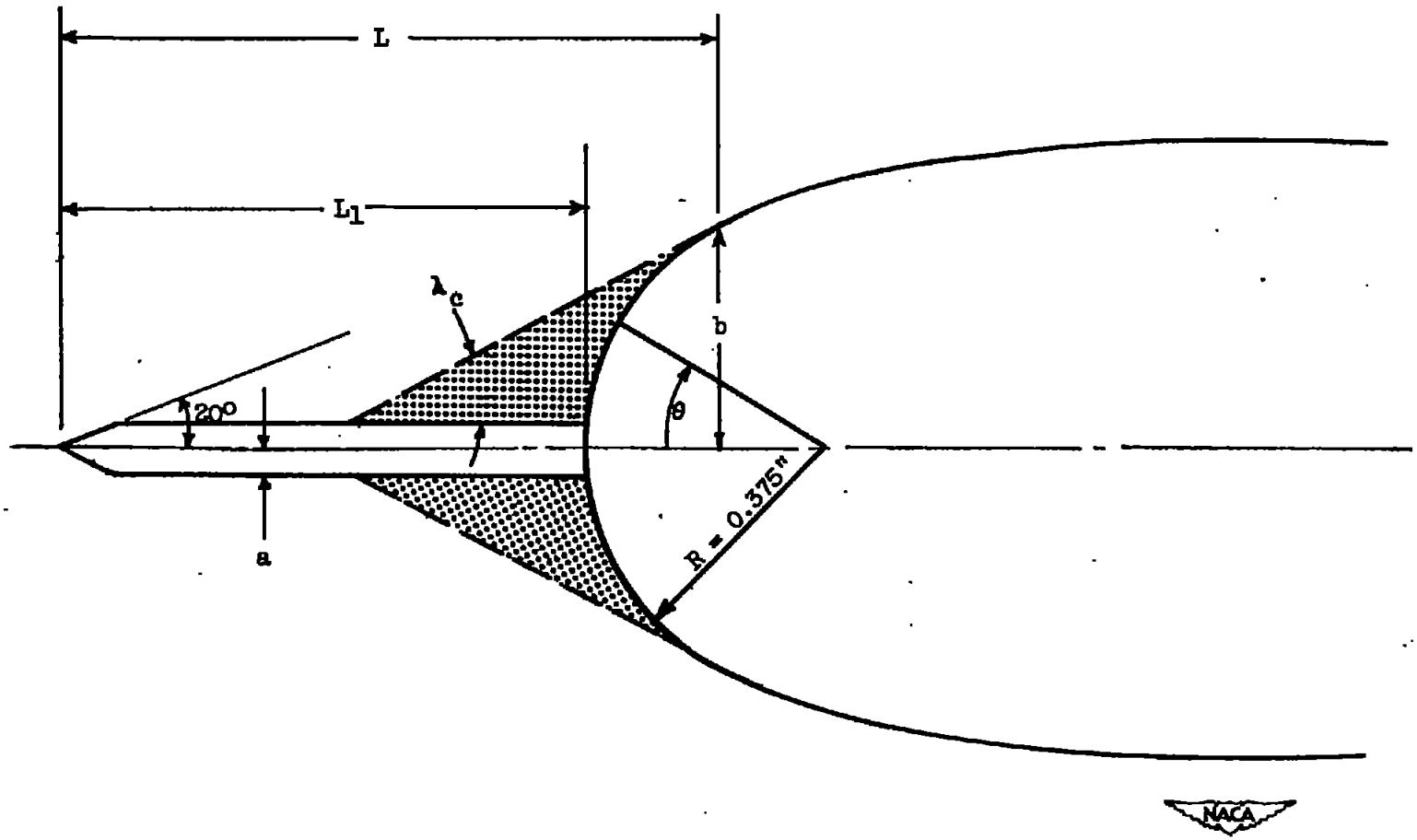

Figure 1. - Notation used and significant dimensions of model.

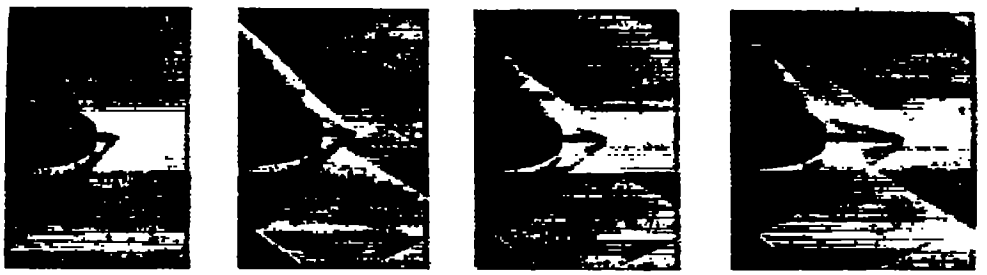

(a) $\frac{R}{L_1} = 1.00$. (b) $\frac{R}{L_1} = 0.70$. (c) $\frac{R}{L_1} = 0.50$. (d) $\frac{R}{L_1} = 0.30$.

(e) $\frac{R}{L_1} = 0.25$. (f) $\frac{R}{L_1} = 0.20$. (g) $\frac{R}{L_1} = 0.15$.

(h) $\frac{R}{L_1} = 0.08$.

NACA C-28322

(i) $\frac{R}{L_1} = 0.04$.

Figure 2. - Effect of tip projection on flow separation with natural transition. $M_0 = 1.93$, $a/R = 0.17$.

[redacted]

(a) $\frac{R}{L_1} = 0.94$. (b) $\frac{R}{L_1} = 0.35$. (c) $\frac{R}{L_1} = 0.30$. (d) $\frac{R}{L_1} = 0.25$.

(e) $\frac{R}{L_1} = 0.20$. (f) $\frac{R}{L_1} = 0.15$. (g) $\frac{R}{L_1} = 0.08$

(h) $\frac{R}{L_1} = 0.06$

NACA C-28323

(i) $\frac{R}{L_1} = 0.04$.

Figure 3. - Effect of tip projection on flow separation with artificial transition. $M_0 = 1.93$, $a/R = 0.17$.

[redacted]

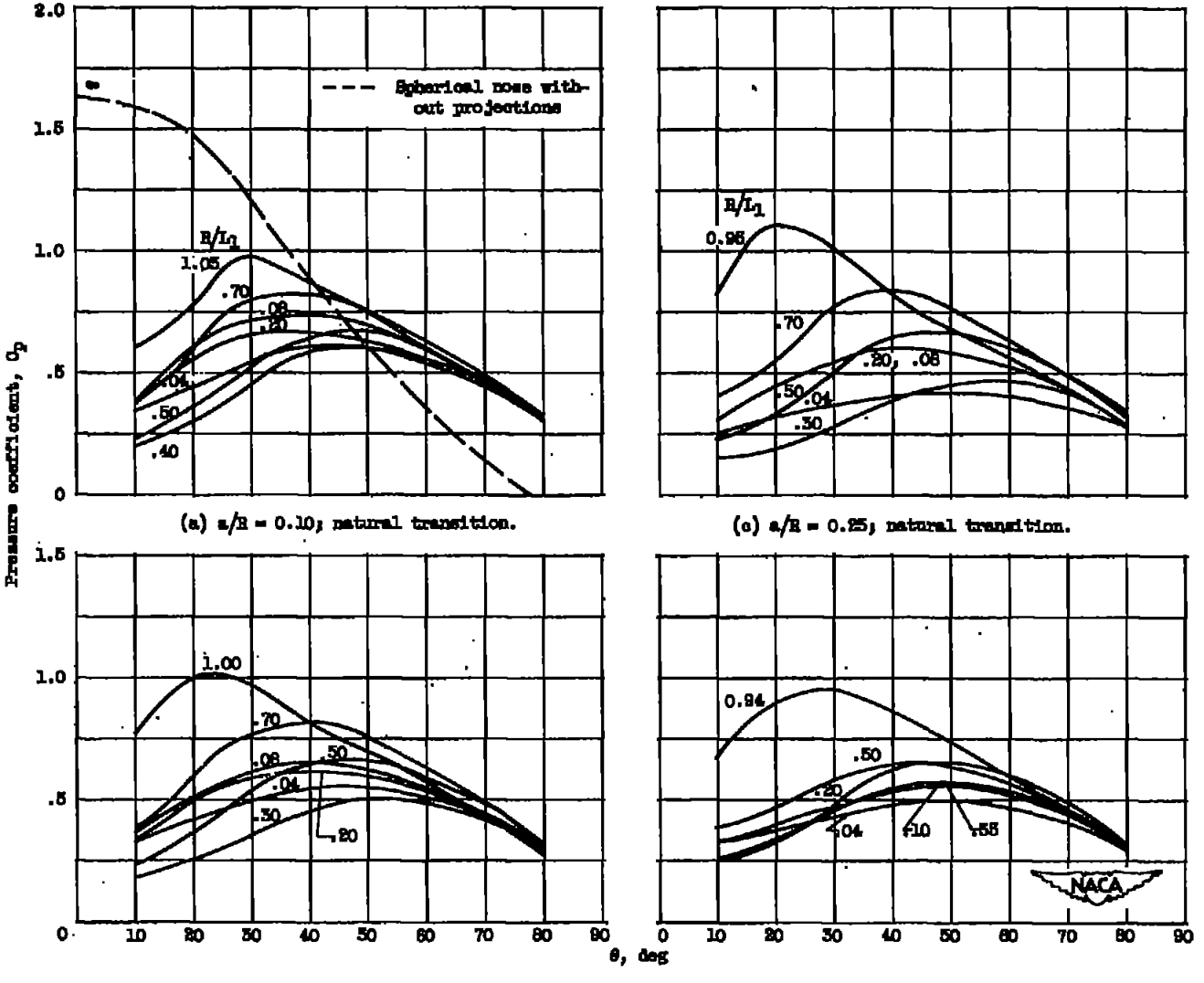

(a) $a/R = 0.10$; natural transition.

(c) $a/R = 0.25$; natural transition.

(b) $a/R = 0.17$; natural transition.

(d) $a/R = 0.17$; artificial transition.

Figure 4. - Pressure distribution as function of tip projection for several rod radii. Mach number M_0, 1.85.

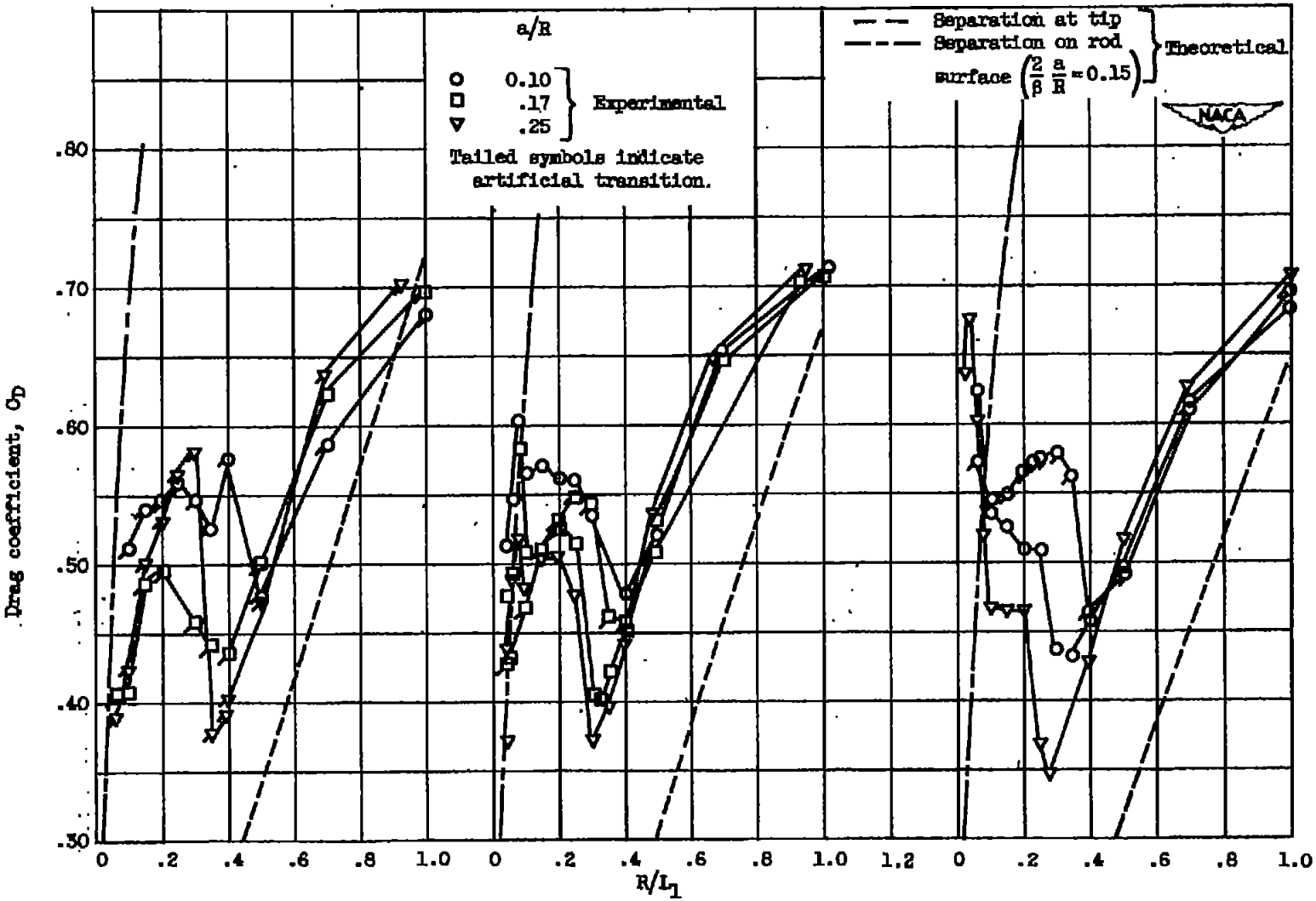

(a) Mach number, M_0, 1.76 (b) Mach number, M_0, 1.93 (c) Mach number, M_0, 2.10

Figure 5. - Drag coefficient of spherical nose as function of tip projection.